Volume 17 | Number 10 | 14 March 2015 | Pages 6671–7078

PCCP

Physical Chemistry Chemical Physics

www.rsc.org/pccp

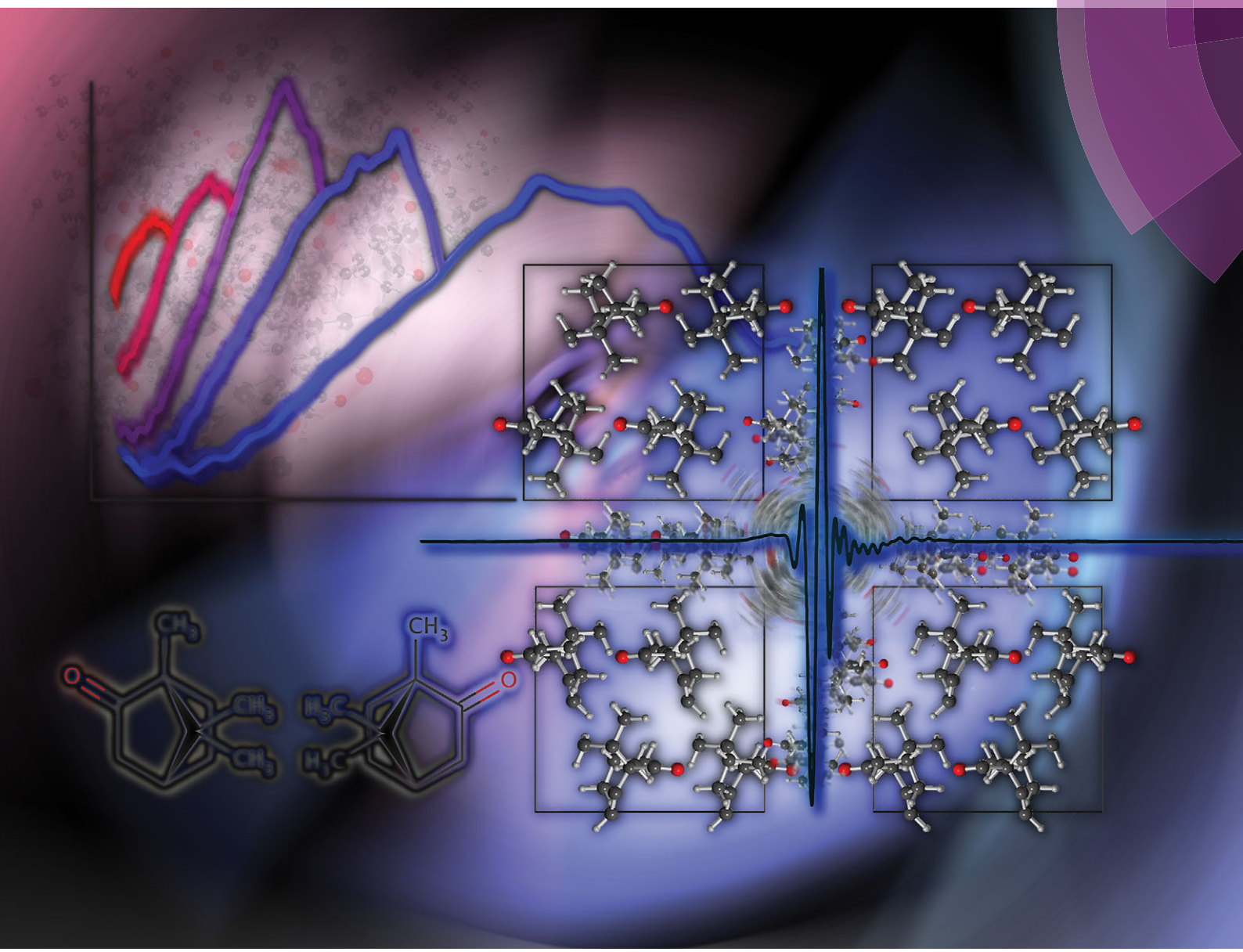

ISSN 1463-9076

ROYAL SOCIETY OF CHEMISTRY

PAPER

Daniel V. Nickel *et al.*

Terahertz disorder-localized rotational modes and lattice vibrational modes in the orientationally-disordered and ordered phases of camphor

PCCP

PAPER

View Article Online
View Journal | View Issue

Cite this: *Phys. Chem. Chem. Phys.*, 2015, **17**, 6734

Terahertz disorder-localized rotational modes and lattice vibrational modes in the orientationally-disordered and ordered phases of camphor

Daniel V. Nickel,*[a] Michael T. Ruggiero,[b] Timothy M. Korter[b] and Daniel M. Mittleman[a]

Received 28th October 2014,
Accepted 26th November 2014

DOI: 10.1039/c4cp04947k

www.rsc.org/pccp

The temperature-dependent terahertz spectra of the partially-disordered and ordered phases of camphor ($C_{10}H_{16}O$) are measured using terahertz time-domain spectroscopy. In its partially-disordered phases, a low-intensity, extremely broad resonance is found and is characterized using both a phenomenological approach and an approach based on *ab initio* solid-state DFT simulations. These two descriptions are consistent and stem from the same molecular origin for the broad resonance: the disorder-localized rotational correlations of the camphor molecules. In its completely ordered phase(s), multiple lattice phonon modes are measured and are found to be consistent with those predicted using solid-state DFT simulations.

1 Introduction

The room temperature bulk condensed phase of camphor, a bicyclic chiral molecule with the general formula $C_{10}H_{16}O$, is considered a plastic-crystal (PC) due to the presence of translational order and orientational disorder: disorder which arises from the dynamic rotation of the translationally-fixed molecules, *i.e.* a rotor phase.[1] This rotational disorder is characteristic of both the crystals containing only right or left-handed enantiomers (homochiral) and of a crystal with a 1 : 1 mixture of both enantiomers (racemic).[2] The similar phase behavior of racemic and homochiral camphor diverges at lower temperatures. Homochiral camphor undergoes a first-order solid-solid phase transition at T_{PC-OC} = 244 K into an orientationally-ordered crystal (OC).[3] Conversely, racemic camphor, at T_{PC-GC} = 190–210 K, undergoes a higher-order transition into a glassy-crystal (GC) phase where its orientational disorder is 'frozen-in', *i.e.* the molecules in its orthorhombic unit cell are each frozen into one of 4 fixed orientations, and the orientation of each molecule is random with respect to that of its neighbors.[4] Therefore, camphor is a rich molecular system that consists of multiple condensed phases with varying permutations of partial disorder and complete order.

Terahertz time-domain spectroscopy (THz-TDS) is uniquely suited to probe the properties of its partially-disordered and ordered phases. It has provided valuable insight into many other disordered materials, such as polymers,[5] glasses,[6–8] and liquids.[9–11] In addition, dynamics universal to disordered materials, including disordered-induced coupling of localized vibrational modes to photons,[12] the Poley peak in liquids,[13] and the Boson peak in amorphous solids,[14] are known to occur in the far-IR and THz range. On the other hand, THz-TDS is also an excellent tool for probing ordered molecular crystals, which often exhibit infrared-active lattice vibrational modes in this spectral range.[15–18] In camphor, neutron scattering measurements of its orientationally-disordered phases have already revealed a curious excess feature in its phonon density of states in the range of 25 to 100 cm^{-1} (0.75–3.0 THz).[19] Additionally, Raman[20] and far-IR[21] studies of homochiral camphors' low-T OC phase(s) have revealed multiple resonance features in the range from 30 to 80 cm^{-1} (0.9–2.4 THz). However, no attempt has been made to assign these features to their specific molecular origins. Therefore, THz-TDS of racemic and homochiral camphor, coupled with solid-state DFT simulations, has the potential to provide valuable fundamental insight into the ordered and partially-disordered phases of this complex soft condensed matter system.

In this study we present the temperature-dependent THz spectra of racemic (RS(±)) and homochiral (R(+) & S(−)) camphor, from frequencies of 0.2 to 2.70 THz and temperatures from 12 K to 340 K. In the orientationally-disordered phases of these three materials, their spectra are virtually indistinguishable, exhibiting a very broad, low intensity absorption peak. In racemic camphor (RS(±)), this feature persists through a solid–solid phase transition into its low-T orientationally-disordered GC phase. This is an indication that the origin of the broad absorption feature is

[a] *Electrical and Computer Engineering Department, Rice University, 6100 Main St., Houston, TX 77005, USA. E-mail: dn4@rice.edu*
[b] *Department of Chemistry, Syracuse University, 1-014 Center for Science and Technology, Syracuse, NY 13244, USA*

related to the presence of disorder and not to dynamical reorientations, which freeze out upon cooling from the PC rotor phase to the GC phase. We characterize the broad feature using both a phenomenological and an *ab initio* approach. In contrast, homochiral camphors' (R(+) or S(−)) low-T OC spectra exhibit multiple lattice phonon modes typical of ordered molecular crystals. These modes are compared and assigned to those predicted using rigorous solid-state density functional theory (DFT) simulations.

2 Experimental details and theory

Homochiral and racemic camphor samples were obtained from Sigma-Aldrich chemicals with purities of 98% for R(+), 99% for S(−), and 96% for RS(±) and used without further purification. The individual molecular structures of the enantiomers are shown in Fig. 1. The initially opaque, soft polycrystalline solids are hand-pressed into transparent discs in the center of Teflon ring spacers, with inner diameters of 4 mm and thicknesses of 600 μm, 300 μm, and 100 μm. The thickness of the Teflon spacers sets the optical path length of the measurements. Two thick (2 mm) high-resistivity Si wafers are placed over the exposed faces of the camphor and Teflon discs, to serve as both windows and thermal contacts for efficient temperature control. The prepared samples are then mounted inside a Cryo-Industries RC-102 cryostat, positioned so the sample rests in the focal plane of the THz beam. THz transients are generated using a custom GaAs photoconductive switch which is gated by 80 fs optical (800 nm) pulses from a Ti:sapphire oscillator, and are measured using electro-optic sampling using a 1 mm thick ZnTe crystal.[22] The THz beam is quasi-optically collimated and focused through the cryostat and the sample using pairs of off-axis parabolic mirrors and Si lenses, respectively. To eliminate water vapor absorption, the entire THz beam path is purged with dry N_2. In order to obtain the sample's indices of refraction, $n(\nu)$, and absorption coefficients, $\alpha(\nu)$, the ratio of the Fourier transforms of the time-domain waveforms transmitted through the sample and through an empty cell reference, *i.e.* the transmission function, is inverted using the thick-film approximation[23] or numerically solved using the Newton–Raphson method.[24] Theoretical fits to the measured spectra were performed using the OriginPro software package which utilizes the Levenberg–Marquardt algorithm.

The solid-state simulations were performed with the CRYSTAL09 software package.[25] Geometry optimizations were performed with energy convergence criterion of 10^{-8} hartree, and the starting atomic positions were taken from the published crystallographic data. While low temperature synchrotron powder X-ray diffraction experiments have been performed on the homochiral species,[3] yielding reliable atomic positions, only disordered powder X-ray diffraction data for the racemic species exists in the literature.[4] The disorder associated with the racemic species led to four possible ordered crystallographic arrangements in the *Cc* space group, and simulations were performed on each form individually. The simulations were performed with the generalized gradient approximation (GGA) Perdew–Burke–Ernzerhof (PBE)[26] density functional. The split-valence double-ζ 6-31G(d,p) basis set was used for all atomic species.[27] Grimme's semi-empirical D-2 London-dispersion correction[28] was used, with the modified van der Waals radii[29] and the s_6 scaling factor set to 0.50. The simulations of the vibrational spectra were performed within the harmonic approximation using the optimized atomic positions, and infrared intensity data was obtained through the Berry phase method.[30] The energy convergence for the frequency analyses was set to 10^{-10} hartree.

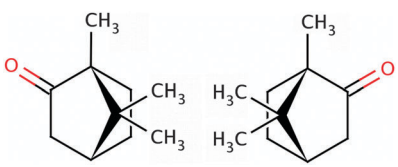

Fig. 1 R(+) (left) and S(−) (right) camphor.

3 Results and discussion

3.1 Terahertz spectra

Plotted in Fig. 2 are $n(\nu)$ and $\alpha(\nu)$ for racemic and homochiral camphor in their PC phases at T = 294 K, and in the GC phase (racemic) and OC phase(s) (homochiral) at T = 12 K. At room temperature their spectra are virtually indistinguishable, displaying a very broad absorption peak with a center frequency,

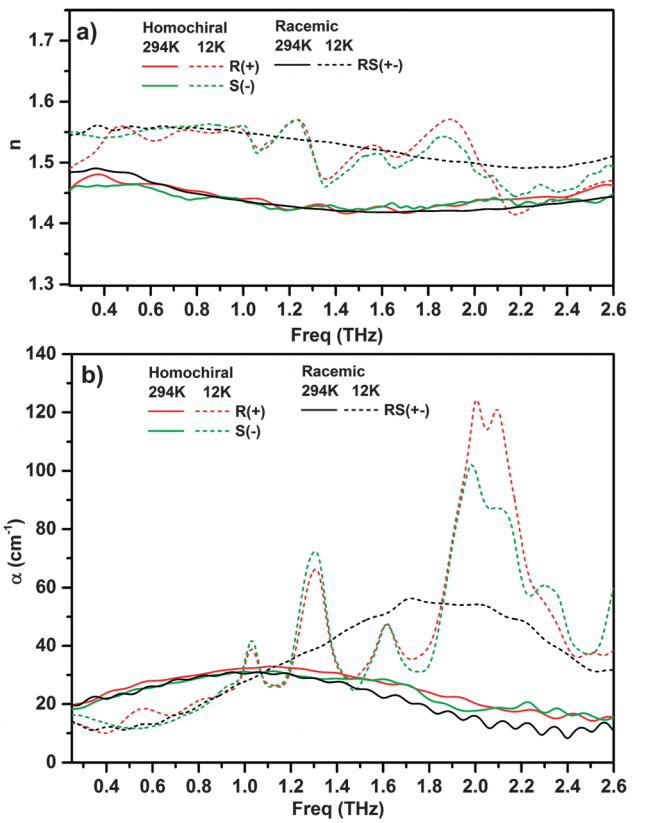

Fig. 2 (a) $n(\nu)$ and (b) $\alpha(\nu)$ for the racemic (black) and homochiral (red, green) camphor samples at T = 294 K (solid) and T = 12 K (dashed).

ν_c, of approximately 36 cm^{-1} (1.1 THz). However, upon cooling through their respective solid–solid phase transitions, racemic and homochiral camphors' spectra become strikingly different. Racemic camphor retains the very broad absorption feature, which shifts continuously to higher frequencies at lower T's. It also becomes slightly asymmetric, with a steeper high frequency wing. Conversely, homochiral camphors' low-T spectra exhibit at least five Lorentzian-like peaks. Considering that the sample at this temperature is orientationally and translationally ordered,[3] these can be attributed *a priori* to lattice vibrational modes, *i.e.*, phonons. The apparent differences in the absorption intensity between the two homochiral samples are due to inconsistencies in sample quality.

3.2 Temperature-dependence of the absorption features

In Fig. 3(a) and (b), the center frequencies, ν_c, of the broad absorption feature and of the five most prominent lattice phonon modes are plotted *vs.* T. The mean ν_c's of the broad absorption feature red-shift with increasing T (Fig. 3(a)). There is significant error in the mean ν_c's between different samples and T's, not surprising given its extremely broad linewidth. Given this uncertainty, racemic camphor's GC to PC phase transition around $T \sim 190$ K is virtually imperceptible in the T-dependence of the ν_c's. However, the phase transition can clearly be distinguished in the temperature-dependent index of refraction (Fig. 3(a) inset). The change in its $\delta n/\delta T$ around $T \sim 195$ K is a clear indication of the GC–PC phase transition, similar to the glass transitions observed in polymers.[5] The phonon modes in the low-T OC phase(s) of homochiral camphor also red-shift with increasing T, typical of lattice modes that are anharmonic[31] (Fig. 3(b)). The modes are qualitatively consistent with those observed in the previously cited Raman[20] and far-IR[21] studies. Above $T \sim 140$ K the two higher frequency modes near 66 cm^{-1} (2 THz) become nearly indistinguishable due to significant broadening, resulting in the increased scatter in their measured ν_c's. The appearances or disappearances of the prominent phonon modes at $T \sim 235$ K in the homochiral camphor samples are consistent with their previously cited phase behavior. Above $T \sim 235$ K, the ν_c's of the broad features in the racemic and homochiral samples are indistinguishable. Curiously, upon heating or cooling racemic camphor through $T \sim 40$ K a repeatable discontinuity in the broad absorption feature's ν_c also appears. This significant shift also coincides with a small discontinuity in $n(\nu)$, usually taken as an indication of a phase transition.[32] However, a previous low-T thermodynamic study shows no sign of a phase transition at this temperature.[33] This discrepancy may be due to a difference in experimental pressures; in this experiment the pressure surrounding the sample is $<10^{-3}$ mbar ($<10^{-5}$ atm), while in the cited reference the stated pressure is 10^5 Pa (0.986 atm). Given the very complex phase diagram of camphor, with at least nine different polymorphs when varying the pressure and temperature,[34] it is possible that this feature near 40 K indicates another as-yet-unidentified low-T, low-P polymorph.

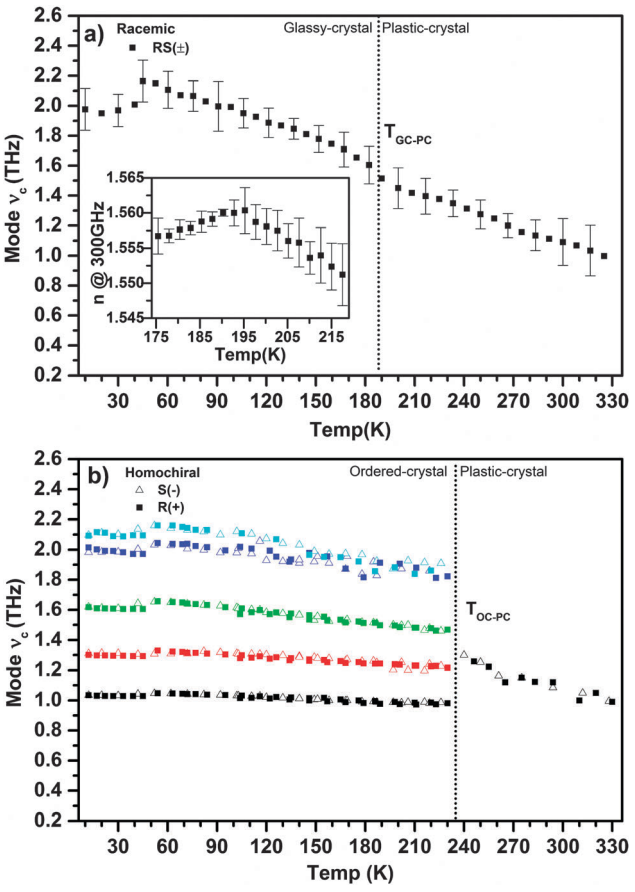

Fig. 3 (a) Plot of the mean center frequencies, ν_c, *vs.* T of the broad absorption feature for 3 different racemic (RS±) camphor samples. Inset of (a): Mean refractive indices, n, at 300 GHz *vs.* T, showing the glass transition at $T \sim 190$–200 K. (b) The ν_c's of the five most prominent phonon modes in the homochiral camphor samples (100 μm thick, R(+) and S(−)) for their OC phases (<235 K) and the ν_c's of the broad absorption features in their PC phases (>235 K). Approximate phase transition T's are demarcated with the dotted lines.

3.3 Origin of the OC phase absorption features

Plotted in Fig. 4 is a representative OC phase spectrum of a 300 μm thick homochiral (S(−)) sample at $T = 100$ K, along with the vibrational modes predicted *via* solid-state DFT simulations. Despite homochiral camphor's complex low-T structure,[3] the simulations reproduce a spectrum very similar to the experiment, predicting 15 IR-active modes with relative intensities comparable to the experimental values. When the modes are convolved with Lorentzians, using the predicted IR intensities and mode-independent FWHM linewidths of 100 GHz, the theoretical absorption spectrum closely resembles the measured one. Given the large number of predicted modes it can be difficult to unambiguously assign them to their experimental counterparts. The predicted modes, IR intensities, and their corresponding molecular motion are given in Table 1.

3.4 Origin of the PC and GC phase absorption feature

The origin of the broad absorption feature in both racemic and homochiral camphors' room-T PC phases and in racemic camphor's low-T GC phase is of particular interest. Its persistence through

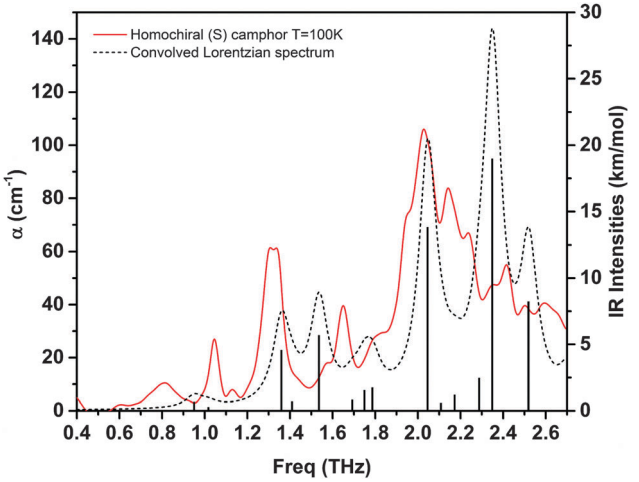

Fig. 4 Comparison of the measured 100 K homochiral (S(−)) spectrum (red line) with the convolved $\Delta\upsilon$ = 100 GHz Lorentzian spectrum using the predicted mode frequencies and intensities (black dotted line). The mode IR intensities are also plotted (columns, right scale). The measured spectrum has been offset by −17 cm^{-1} to zero.

Table 1 DFT predicted mode frequencies, IR intensities, and assignments for homochiral camphor in its OC phase

Frequency (THz)	Wavenumber (cm^{-1})	Intensity (km mol^{-1})	Motion
0.9505	31.71	0.65	Rotation about *c*
1.017	33.93	0.26	Translation in *c*
1.359	45.35	4.56	Rotation about *a*
1.409	47.03	0.68	Rotation about *a*
1.536	51.24	5.68	Rotation about *c*
1.692	56.46	0.82	Rotation about *b*
1.748	58.34	1.54	Rotation about *c*
1.786	59.58	1.74	Translation in *b*
2.045	68.22	13.81	Rotation about *a*
2.108	70.33	0.58	Rotation about *b*
2.172	72.46	1.19	Rotation about *c*
2.287	76.31	2.46	Rotation about *c*
2.348	78.35	18.98	Rotation about *a*
2.510	84.02	8.22	Rotation about *a*
2.704	90.20	1.84	Rotation about *c*

racemic camphor's PC-to-GC phase transition would seem to preclude the possibility of attributing it to long-range phonon mode(s) since, in addition to the presence of orientational disorder in both phases, the structure of the PC and GC phases are not equivalent; its PC phases have a hexagonal unit cell,[2] while its GC phase unit cell is orthorhombic.[4] Additionally, earlier dielectric measurements have shown a Debye relaxation time of ~20 ps or slower at room temperature for the PC phase.[35–37] This would result in a resonance outside of our accessible frequency window, and moreover it is not observed in racemic camphor's low-*T* GC phase. Therefore the measured absorption feature can not be attributed to the same Debye reorientational process observed in the dielectric studies. The dynamic process behind the measured THz feature is more than an order of magnitude faster; hence it must arise from a different molecular origin. To explore its origin, we take two approaches. The first is a phenomenological approach which stems from the characterization of completely disordered materials, including polar and non-polar liquids. The second is a computational approach which relies upon *ab initio* DFT simulations of four possible permutations of racemic camphor's GC phase unit cell.

To phenomenologically characterize dipolar correlations in condensed phase disordered materials in the far-IR range, Mori's continued fraction formalism is often used.[38] This approach stems from the generalized Langevin equation and the dipole correlation function, and has been used to characterize the far-IR absorption (the so-called Poley peak) in non-dipolar liquids[39,40] and, more recently, a Boson peak in the rotor-phases of *n*-alkanes.[32] Past investigations of other orientationally-disordered PC's, such as tertiary butyl-chloride[41] and methyl-chloroform,[42] have suggested their far-IR spectra can be attributed to short-range correlated vibrations similar to the origin of the Poley peak in liquids, even in these cases where there is complete translational order but orientational disorder. The Poley peak's physical origin has been attributed to gyroscopic orientational oscillations (librations) of a molecule's permanent and/or induced dipole moment. In a simple itinerant oscillator model, the frequency of this libration is proportional to that of a rigid rotor, $(kT/I)^{1/2}$.[43] Camphor has a non-zero dipole moment,[44] so these dipolar librations could couple to the probing THz radiation. Using this approach, the experimental observables, $n(\omega)$ and $\alpha(\omega)$, can be related to the second order expansion of the Mori memory kernel using:[13,38]

$$\alpha(\omega)n(\omega) = \frac{\Delta\varepsilon}{c}\frac{\gamma K_1 K_2}{\gamma^2(K_1-\omega^2)+\omega^2(\omega^2-K_1-K_2)^2} \quad (1)$$

Ideally, the parameter K_1 can be related to dipolar angular momentum while K_2 and γ can be related to the amplitude and damping constant of the intermolecular torque correlation decay function, $K_2(t) = K_2 e^{-\gamma t}$.

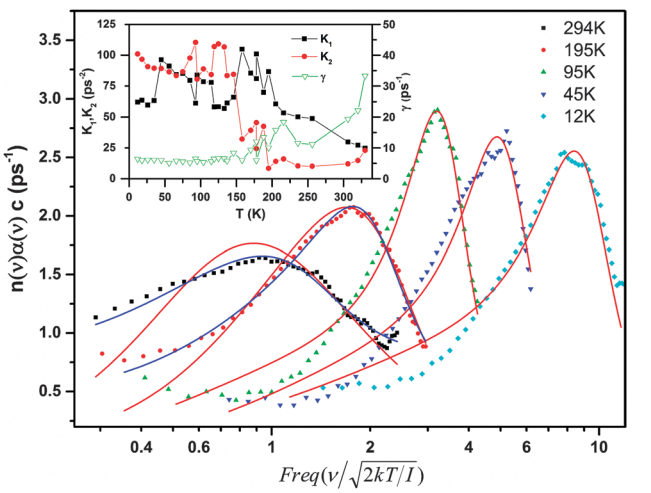

Fig. 5 The combined, $n(\nu)\alpha(\nu)$c, spectra of racemic camphor plotted *vs.* their reduced frequencies at a few different *T*'s. Fits to eqn (1) (red lines) and eqn (1) with the Debye relaxation offset (blue lines) are also plotted. Inset: The extracted fit parameters K_1, K_2 and γ *vs.* *T*.

Plotted in Fig. 5 are the fits of eqn (1) to a few representative spectra, with their frequencies normalized by camphor's rigid rotor frequencies approximated as a symmetric top, $(2kT/I)^{1/2}$.[45] With the known values of $\Delta\varepsilon(T)$[35] and K_1, K_2, and γ as free parameters, the fits of eqn (1) to racemic camphor's low-T GC phase ($T < 190$ K) spectra are satisfactory; it reproduces the measured spectra well in the region of the peaks but deviates on their low frequency wings. However, eqn (1) begins to fail for $T > 190$ K, demonstrated by the less than satisfactory fits of the $T = 195$ K and $T = 294$ K spectra in Fig. 5. With inclusion of an additional $n(0)\alpha(0)$ additive offset parameter, the higher-T PC phase spectra can also be satisfactorily reproduced. Physically, this offset, which increases as T increases, can be attributed to the encroaching high-frequency wing of camphor's PC phase Debye relaxation.[35–37] Plotted in the inset are the extracted parameters K_1, K_2, and γ from the fits over the entire range of T's. The two intermolecular torque correlation parameters K_2 and γ remain relatively constant in racemic camphor's low-T GC phase, but then begin to decrease and slowly increase, respectively, as T approaches and passes T_{GC-PC}. The parameter K_1, with the exceptions of the anomalous and expected phase transitions, decreases approximately linearly with T. We can qualitatively compare our normalized fit parameters (normalized using $(2kT/I)^{1/2}$ for γ and $(2kT/I)$ for K_1, K_2) to the results of Davies and Evans[13] for several different molecules in their bulk liquid phases. Interestingly, camphor's K_2 parameters in its GC and PC phases (practically equivalent to each other) are almost an order of magnitude smaller compared to the liquids, *i.e.* relative to the liquids its mean squared intermolecular torque is initially more weakly correlated, which is reasonable given its translational order. The K_1 and γ parameters are comparable to the liquids in its PC phase ($T = 294$) but are an order of magnitude less in its low-T GC phase ($T = 12$ K), corresponding to a significant decrease in both the dipolar angular momentum and in the damping of the correlations. Hence with reduced temperature its rotational/librational dynamics are slowed and remain correlated for a longer period of time. From γ, the lifetime of these correlation are $\sim$0.2 ps and $\sim$0.06 ps in its GC ($T = 12$ K) and PC ($T = 294$ K) phases, respectively. The satisfactory fits of the spectra to eqn (1) support the hypothesis that the broad feature originates from correlated dipolar motion, following the correlation function derived in Davies and Evans.[13]

As an alternative approach to analyzing the broad absorption feature, we can use *ab initio* density functional theory. We simulate the four known arrangements of racemic camphor's GC phase *Cc* unit cells, treating each as a separate orientationally-ordered single-crystal. These four variations are symmetry unique, but extremely close in energy to one another (Gibbs free energy differences of <1 kJ mol^{-1}) so that unambiguous identification of the most stable form is not appropriate. The simulations of each of the separate arrangements predict the presence of ≤ 8 IR-active modes in this spectral range. Since each unit cell in the sample contains randomly oriented molecules representing one of these four possible orientations, it is reasonable to assume that the measured spectrum could be predicted by superposing the four independently calculated spectra. The superimposed modes of the four 'single-crystal' configurations are plotted in Fig. 6 along with the

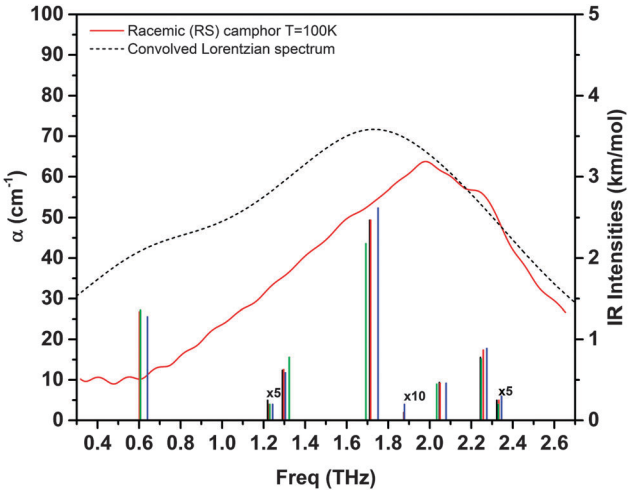

Fig. 6 The measured absorption spectrum of a 600 μm racemic camphor sample at $T = 100$ K (red line) plotted with the combined spectrum using the DFT predicted modes from its four GC phase 'single-crystal' unit cells (each broadened using a Lorentzian with a broadening factor of $\Delta\upsilon = 600$ GHz) (black dotted line). Also plotted are the mode IR intensities for all four unit cells (columns, right scale).

spectrum of the 600 μm thick racemic camphor sample at $T = 100$ K. The modes from the different arrangements, which group together in the spectrum with similar ν_c's, arise from identical molecular rotations about their crystallographic axes. In order of increasing frequency, the predicted modes correspond to the following rotations: about *a*, about *b*, about *c*, about *a*, in *bc* plane, in *ab* plane, about *abc*, and about *b*. The theoretical rotational modes, superimposed in the same spectrum, physically represent a theoretical polycrystal which consists of extended orientationally-ordered single crystal domains of camphor's four simulated GC configurations. In reality, however, camphor's orientational disorder is much more homogeneously distributed. This increased nano-scale disorder relative to the theoretical polycrystal would manifest itself in the experimental spectra through broadening of the mode linewidths, $\Delta\upsilon$. With this in mind, we convolve the modes with Lorentzians using their predicted IR intensities and equal $\Delta\upsilon$'s of 20 cm^{-1}. This theoretical spectrum is plotted in Fig. 6 along with a representative experimental spectrum. In this case the predicted modes can closely mimic the experimental spectrum when significant broadening is included. With $\Delta\upsilon$'s of 20 cm^{-1} (0.6 THz), we can make an order of magnitude estimate of the coherence length of the vibrations contributing to the broad spectral feature. A FWHM linewidth of 0.6 THz corresponds to a lifetime of $\sim$0.3 ps. Using the speed of sound in camphene ($\sim$1500 m s^{-1}) (a similar plastic-crystal),[46] this lifetime correspond to a coherence length of only $\sim$0.4 nm, which is roughly the size of a single camphor molecule. If the broad feature does originate from the superposition of these predicted 'single-crystal' modes, the extreme broadening in the experimental spectra is undoubtedly a result of racemic camphor's inherent orientational disorder. We have confirmed experimentally that this disorder is intrinsic to the sample by annealing a racemic crystal at T_{GC-PC} for 144 h. In spite of the annealing process, no change was observed in its low-T spectra.

4 Conclusions

In the partially-disordered phases of this soft matter, both the phenomenological and computational approach characterize the behavior of its THz absorption spectrum. In both cases, we are led to the same conclusion for the molecular origin: the correlated rotation/libration of the molecules. Both approaches also lead to nearly the same estimated lifetime for these correlations of about 0.2–0.3 ps. This time constant is nearly two orders of magnitude faster than previously characterized Debye processes in this material, suggesting a different molecular origin. Since the dynamics are disorder-localized and purely rotational, they can persist through the PC to GC phase transition despite the different structures and the 'freezing-in' of its dynamic orientational disorder. The intermediary nature of the disorder in the PC and GC phases of camphor pose an interesting question concerning what terminology to use to label this broad feature. It is tempting to label it as a Poley or Boson peak, given the satisfactory fits to eqn (1), the evidence for disorder-localized modes, and the past studies of disordered solids and other PC's. It has been suggested both the Boson peak and Poley peak arise from the same underlying molecular origin.[47] Both labels, however, have historically only been used for the anomalous far-IR peaks found in amorphous solids and liquids. In addition, the Boson peak has traditionally been described as an excess in the Debye acoustic vibrational density of states, modes which normally would not couple to optical excitations. However, it is well known that the presence of disorder breaks down the selection rules preventing far-IR optical excitation of acoustic modes[12] and studies have shown that the Boson peak can consist of both acoustic and/or non-acoustic contributions.[48–50] And, indeed, a similar far-IR feature in *ortho*-carborane, another orientationally-disordered molecular PC, has been labeled as a Boson peak, with its origin attributed to the coupling of IR-active phonon-like modes to localized vibrational modes.[51] While it may be presumptuous to label camphor's THz range broad absorption feature as a Boson peak or Poley peak, it certainly could be their analogue in this partially-disordered molecular system.

Acknowledgements

This research was funded in part by the R. A. Welch Foundation and by a grant from the National Science Foundation (CHE-1301068).

References

1 *The Plastically Crystalline State*, J. N. Sherwood, John Wiley and Sons, New York, 1979.
2 C. C. Mjojo, *J. Chem. Soc., Faraday Trans. 2*, 1979, **75**, 692.
3 M. Brunelli, A. N. Fitch and A. J. Mora, *J. Solid State Chem.*, 2002, **163**, 253.
4 A. J. Mora and A. N. Fitch, *J. Solid State Chem.*, 1997, **134**, 211.
5 S. Wietzke, C. Jansen, T. Jung, M. Reuter, B. Baudrit, M. Bastian, S. Chatterjee and M. Koch, *Opt. Express*, 2009, **17**, 19006–19014.
6 M. Zalkovskij, C. B. Zoffmann, A. Novitsky, R. Malureanu, D. Savastru, A. Popescu, P. U. Jepsen and A. V. Lavrinenko, *Appl. Phys. Lett.*, 2012, **100**, 031901.
7 A. Podzorov and G. Gallot, *Chem. Phys. Lett.*, 2010, **495**, 46.
8 M. Naftaly and R. E. Miles, *J. Appl. Phys.*, 2007, **102**, 043517.
9 L. Thrane, R. H. Jacobsen, P. U. Jepsen and S. R. Keiding, *Chem. Phys. Lett.*, 1995, **240**, 330.
10 P. Laib and D. M. Mittleman, *J. Infrared, Millimeter, Terahertz Waves*, 2010, **31**, 1015.
11 J. T. Kindt and C. A. Schmuttenmaer, *J. Phys. Chem.*, 1996, **100**, 10373.
12 S. N. Taraskin, S. I. Simdyankin, S. R. Elliot, J. R. Neilson and T. Lo, *Phys. Rev. Lett.*, 2006, **97**, 055504.
13 G. J. Davies and M. Evans, *J. Chem. Soc., Faraday Trans. 2*, 1976, **72**, 1194.
14 W. A. Phillips, *Amorphous solids: low-temperature properties*, Springer, New York, 1981.
15 D. G. Allis, D. A. Prokhorova and T. M. Korter, *J. Phys. Chem. A*, 2006, **110**, 1951–1959.
16 K. Kawase, Y. Ogawa, Y. Watanabe and H. Inoue, *Opt. Express*, 2003, **11**, 2549.
17 P. U. Jepsen and S. J. Clark, *Chem. Phys. Lett.*, 2007, **442**, 275.
18 D. V. Nickel, S. P. Delaney, H. Bian, J. Zheng, T. M. Korter and D. M. Mittleman, *J. Phys. Chem. A*, 2014, **118**, 2442–2446.
19 K. Holderna-Natkaniec, I. Natkaniec, S. Habrylo and J. Mayer, *Physica B*, 1994, **194–196**, 369–370.
20 G. R. Wilkinson, J. A. Medina and W. F. Sherman, *J. Raman Spectrosc.*, 1981, **10**, 155.
21 R. Ramnarine, W. F. Sherman and G. R. Wilkinson, *Infrared Phys.*, 1981, **21**, 391.
22 Q. Wu and X. C. Zhang, *Appl. Phys. Lett.*, 1995, **67**, 3523.
23 Y. S. Lee, *Principles of Terahertz Science and Technology*, Springer, New York, 2009.
24 A. J. Garcia, *Numerical Methods for Physics*, Prentice Hall, New Jersey, 2000.
25 R. O. R. Dovesi, B. Civalleri, C. Roetti, V. R. Saunders and C. M. Zicovich-Wilson, *Crystal09*, University of Torino, Torino, 2009.
26 J. P. Perdew, A. Ruzsinszky, G. I. Csonka, O. A. Vydrov, G. E. Scuseria, L. A. Constantin, X. Zhou and K. Burke, *Phys. Rev. Lett.*, 2008, **100**, 136406.
27 R. Krishnan, J. S. Binkley, R. Seeger and J. A. Pople, *J. Chem. Phys.*, 1980, **72**, 650–654.
28 S. Grimme, *J. Comput. Chem.*, 2004, **25**, 1463–1473.
29 B. Civalleri, C. M. Zicovich-Wilson, L. Valenzano and P. Ugliengo, *CrystEngComm*, 2008, **10**, 405–410.
30 Y. Noel, C. M. Zicovich-Wilson, B. Civalleri, P. D'Arco and R. Dovesi, *Phys. Rev. B: Condens. Matter Mater. Phys.*, 2001, **65**, 014111.
31 S. Dexheimer, *Terahertz Spectroscopy: Principles and Applications*, CRC, Boca Raton, 2008.
32 J. P. Laib, D. V. Nickel and D. M. Mittleman, *Chem. Phys. Lett.*, 2010, **493**, 279.
33 T. Nagumo, T. Matsuo and H. Suga, *Thermochim. Acta*, 1989, **139**, 121.

34 P. W. Bridgeman, *The Physics of High Pressure*, G. Bell and Sons, London, 1958.
35 D. E. Williams and C. R. Smyth, *J. Am. Chem. Soc.*, 1962, **84**, 1808.
36 V. Rossiter, *J. Phys. C: Solid State Phys.*, 1972, **5**, 1969.
37 C. Clement and M. Davies, *Trans. Faraday Soc.*, 1962, **58**, 1718.
38 *Advances in Chemical Physic Volume LVIs*, ed. I. Prigogine and S. A. Rice, John Wiley and Sons, 1984.
39 J. E. Pederson and S. R. Keiding, *IEEE J. Quantum Electron.*, 1992, **28**, 2518.
40 B. N. Flanders, R. A. Cheville, D. Grischowsky and N. F. Scherer, *J. Phys. Chem.*, 1996, **100**, 11824.
41 C. Brot, B. Lassier, G. W. Chantry and H. A. Gebbie, *Spectrochim. Acta*, 1967, **24**, 295.
42 B. Lassier, C. Brot, G. W. Chantry and H. A. Gebbie, *Chem. Phys. Lett.*, 1969, **3**, 96.
43 N. E. Hill, *Proc. Phys. Soc., London*, 1963, **82**, 723.
44 Z. Kisiel, O. Desyatnyk, E. Bialkowska-Jaworska and L. Pszczolkowski, *Phys. Chem. Chem. Phys.*, 2003, **5**, 820.
45 M. Jauquet and P. Laszlo, *Chem. Phys. Lett.*, 1972, **15**, 600.
46 J. R. Green and C. E. Scheie, *J. Phys. Chem. Solids*, 1967, **28**, 383.
47 G. P. Johari, *J. Non-Cryst. Solids*, 2002, **114**, 307–310.
48 B. Ruffle, D. a. Parshin, E. Courtens and R. Vacher, *Phys. Rev. Lett.*, 2008, **100**, 015501.
49 B. Hehlen, E. Courtens, R. Vacher, A. Yamanaka, M. Kataoka and K. Inoue, *Phys. Rev. Lett.*, 2008, **100**, 015501.
50 E. Duval, A. Mermet and L. Saviot, *Phys. Rev. B: Condens. Matter Mater. Phys.*, 2007, **75**, 024201.
51 P. Lunkenheimer and A. Loidl, *J. Non-Cryst. Solids*, 2006, **352**, 4556.

